FEBS Letters 431 (1998) 250–254 FEBS 20528

Three-dimensional structure of binase in solution

M.Ya. Reibarkh, D.E. Nolde, L.I. Vasilieva, E.V. Bocharov, A.A. Shulga, M.P. Kirpichnikov, A.S. Arseniev*

Shemyakin - Ovchinnikov Institute of Bioorganic Chemistry, Russian Academy of Sciences, ul. Miklukho-Maklaya, 16/10, Moscow 117871, Russia

Received 10 June 1998

Abstract We present the spatial structure of binase, a small extracellular ribonuclease, derived from ^{1}H-NMR* data in aqueous solution. The total of 20 structures were obtained via torsion angle dynamics using DYANA program with experimental NOE and hydrogen bond distance constraints and ϕ and χ^1 dihedral angle constraints. The final structures were energy minimised with ECEPP/2 potential in FANTOM program. Binase consists of three α-helices in N-terminal part (residues 6–16, 26–32 and 41–44), five-stranded antiparallel β-sheet in C-terminal part (residues 51–55, 70–75, 86–90, 94–99 and 104–108) and two-stranded parallel β-sheet (residues 22–24 and 49–51). Three loops (residues 36–39, 56–67 and 76–83), which play significant role in biological functioning of binase, are flexible in solution. The differences between binase and barnase spatial structures in solution explain the differences in thermostability of binase, barnase and their hybrids.

© 1998 Federation of European Biochemical Societies.

Key words: Ribonuclease; Binase; NMR; Protein structure

1. Introduction

Binase is a small (M_r 12.1 kDa) extracellular guanylospecific ribonuclease produced by *Bacillus intermedius* [1]. Binase as well as its homologue barnase (the sequential homology of 85%) from *Bacillus amyloliquefaciens* [2] is inhibited by a protein barstar. Barstar strongly interacts with binase and barnase but dissociation constants of the complexes have an approximately two order difference [3,4]. Catalytic constants of binase and barnase are also significantly different [5]. The detailed comparison of binase and barnase spatial structures in solution could explain why so homologous proteins highly differ in catalytic constants and in dissociation constants of their complexes with barstar. These complexes are convenient models for studying the molecular aspects of protein-protein interaction and for understanding the specificity of enzyme-substrate and enzyme-inhibitor interactions. So far the structures of barnase (in crystal [6,7] and in solution [8]), barstar in solution [9], and of barnase-barstar complex in crystal [10], have been determined, and crystal structures of wild-type binase (resolution 3.2 Å) and of H101N binase mutant (resolution 2.2 Å) have been obtained [11,12].

Previously [13] we reported ^{1}H resonance assignment and secondary structure of binase based on the sequential NOEs, secondary chemical shift indexes, hydrogen-deuterium exchange data, and HN-C$^\alpha$H spin-spin coupling constants. Here we present the high-resolution structure of binase in solution and compare it with binase crystal and barnase solution and crystal structures.

2. Materials and methods

2.1. Protein expression and sample preparation

Binase was expressed in *E. coli* XL1 strain [14] and then purified as described in [13]. Lyophilised protein was dissolved in 20 mM potassium phosphate buffer (pH 6.7) and purified from paramagnetic ions by electrodialysing against the same buffer. Sample was concentrated in an Amicon cell with UM-2 membrane to 10 mg in 500 μl of the buffer and then 100 μl of ^2H_2O was added yielding a final protein concentration of approximately 1.5 mM. The sample was lyophilised and dissolved in ^2H_2O for NMR experiments in ^2H_2O.

2.2. NMR measurements

All NMR experiments were performed on Varian Unity 600 spectrometer. NOESY [15] spectra with mixing time (τ_m) of 40, 100 and 200 ms and DQF-COSY [16] spectra were recorded in H_2O and ^2H_2O. All 2D spectra were recorded in the phase-sensitive mode at 30°C with relaxation delay of 1.2 s. The water signal was suppressed by WATERGATE [17] in the NOESY experiments in H_2O and by continuous irradiation during the relaxation delay in the DQF-COSY experiment in H_2O.

2.3. Distance constraints

Proton resonance assignments of binase were reported previously [13]. Assigning of cross-peaks in NOESY spectra and measuring of their volumes were performed using XEASY program [18]. To avoid spin diffusion effect NOESY spectra with mixing time of 40 ms were used to derive distance constraints. Upper interproton distance constraints were calculated from NOE cross-peak volumes, which relative errors [18] were less than 0.1, using CALIBA subroutine in DYANA program [19].

35 NH protons, which signals were detected in spectra recorded at 8 h after protein solubilisation in ^2H_2O, were supposed to be involved in hydrogen bonding. The acceptors of hydrogen bonds were found from the pattern of NOE connectivities between β-strands and from the analysis of preliminary set of 20 structures. Hydrogen bonds were constrained when they were observed in at least 80% of preliminary structures. Eight distance constraints were introduced for 29 backbone-backbone hydrogen bonds to satisfy distance and angle criteria for hydrogen bonds [20]: four upper (3.3, 2.3, 4.6, 3.6 Å) and four lower (3.0, 1.9, 4.2, 3.2 Å) for O...N, O...HN, C...N, and C...HN distances, respectively. For two hydrogen bonds between backbone amide groups and side-chain oxygens (Ile-50 HN-C$^\gamma$O Asp-74 and Leu-94 HN-O$^\gamma$ Ser-90) were introduced four distance constraints – two upper: HN...O 2.3 Å and N...O 3.2 Å, and two lower: HN...O 1.9 Å and N...O 2.8 Å [21].

2.4. Angle constraints

HN-C$^\alpha$H spin-spin coupling constants were determined by the INFIT program [22] analysis of nonoverlapped NOE cross-peaks between corresponding amide proton at ω_2 frequency and aliphatic proton of a neighbouring residue. HC$^\alpha$-C$^\beta$H spin-spin coupling constants for Val, Ile, and Thr residues were determined by the INFIT program analysis of nonoverlapped NOE cross-peaks between corresponding C$^\alpha$H proton at ω_2 frequency and aliphatic proton of a neighbouring

*Corresponding author. Fax: +7 (95) 335-50-33.
E-mail: aars@nmr.ru

Abbreviations: NMR, nuclear magnetic resonance; 2D, two-dimensional; NOE, nuclear Overhauser effect; DQF-COSY, 2D double quantum filtered correlated spectroscopy; NOESY, 2D NOE-correlated spectroscopy; TAD, torsion angle dynamics; PDB, Brookhaven Protein Data Bank; rmsd, root mean square deviation

0014-5793/98/$19.00 © 1998 Federation of European Biochemical Societies. All rights reserved.
PII: S0014-5793(98)00765-0

Table 1
Analysis of the 20 best DYANA and FANTOM binase structures

Parameter	Quantity	DYANA	FANTOM
target function (Å^2)		1.17 ± 0.03	
energy (kcal/mol)			−702 ± 6
no. of distance constraints (upper/lower)	NOE	903/0	903/0
	H-bond	120/120	120/120
no. of torsion constraints	ϕ angle	75	75
	χ^1 angle	38	38
upper constraint violations (Å)	> 0.2 Å	0.3 ± 0.1	0
	maximum	0.24	0.15
lower constraint violations (Å)	> 0.2 Å	0	1.5 ± 0.3
	maximum	0.14	0.24
van der Waals constraint violations (Å)	> 0.2 Å	1.2 ± 0.1	0
	maximum	0.48	0.16
angle constraint violations (deg)	> 3°	0.1 ± 0.1	0
	maximum	3.0	1.7
rmsd of residues (Å):			
1–109	backbone	1.14 ± 0.22	1.25 ± 0.18
	all heavy atoms	1.89 ± 0.22	2.05 ± 0.22
3–35, 40–55, 68–75, 84–109	backbone	0.47 ± 0.12	0.65 ± 0.13
	all heavy atoms	1.23 ± 0.15	1.37 ± 0.16

residue in NOESY spectrum recorded in ^2H_2O. HC^{α}-$C^{\beta}H$ spin-spin coupling constants for the residues containing two chemically unequivalent $C^{\beta}H$ protons were calculated from the DQF-COSY spectrum recorded in ^2H_2O. An active constant of $C^{\alpha}H/C^{\beta}H$ cross-peak was estimated by measuring antiphase splitting and the passive one was calculated by in-phase doublet analysis via the INFIT program.

Angles ϕ were constrained by the crossing of the regions allowed for angle ϕ from the coupling constant [23] and from the intraresidual and sequential NOE cross-peaks. If NOE data were insufficient to bound the ϕ angle it was not restricted at all.

Stereospecific assignment and χ^1 angle constraints were obtained by standard method [24] using intraresidual and sequential NOEs and HC^{α}-$C^{\beta}H$ spin-spin coupling constants.

2.5. Structure calculation

Structures were calculated by using simulated annealing procedure in DYANA program [19]. X-Pro peptide bonds were considered as *trans* being proved with characteristic NOE pattern. A calculating strategy consists of four steps:

1. Generating of an initial structure set basing on unambiguously assigned NOE cross-peaks and unambiguously determined angle ϕ ranges.

2. Iterative reassigning of ambiguous and overlapped NOE cross-peaks using calculated at previous step structures and generation of new structures set, which accounts for new distance and angle constraints.

3. Stereospecific assignment and χ^1 dihedral angle constraints cal-

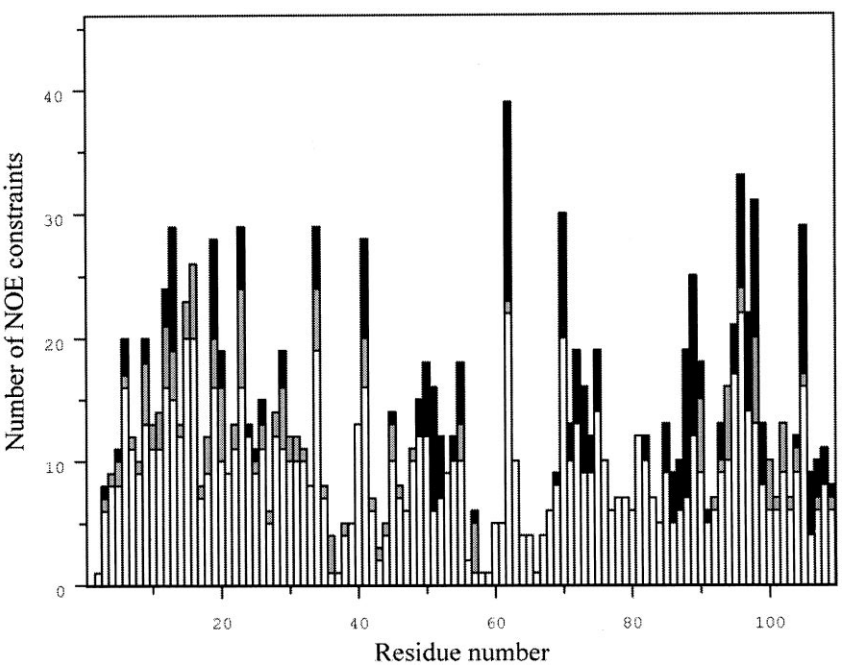

Fig. 1. Histogram of number of NOE constraints for binase residues by ranges: open bars, intraresidual and sequential constraints; gray bars, medium-range (2–5 residues apart) constraints; and black bars, long-range (more than five residues apart) constraints.

culation as well as determination of hydrogen bond acceptors using the preliminary structure set obtained at step 2.

4. Calculation of a final set of structures using all constraints summarised in Table 1.

The default DYANA simulated annealing protocol [19] with 5000 steps of high-temperature TAD and 200 steps of zero-temperature TAD [19] followed by conjugate gradient minimisation was applied to 100 random structures. Resulted 20 structures were chosen from 100 obtained according to their standard DYANA target function [19] values.

Constrained energy minimisation of the 20 best DYANA structures was performed in the FANTOM program [25] using ECEPP/2 potential. The contribution of electrostatic interactions to the conformational energy was calculated with a dielectric constant proportional to the distance between interacting atoms. A pseudoenergy term was introduced for distance and torsion angle constraints to avoid the structure 'drift' from the experimental data. Pseudo-force-field constants were taken equal to 3.2×10^7 kT/Å^6 for distance constraint violations and kT/2 degrees for angle constraint violations. A 1000 step Raphson-Newton minimisation was performed yielding structures with the energy of -702 ± 6 kcal/mol.

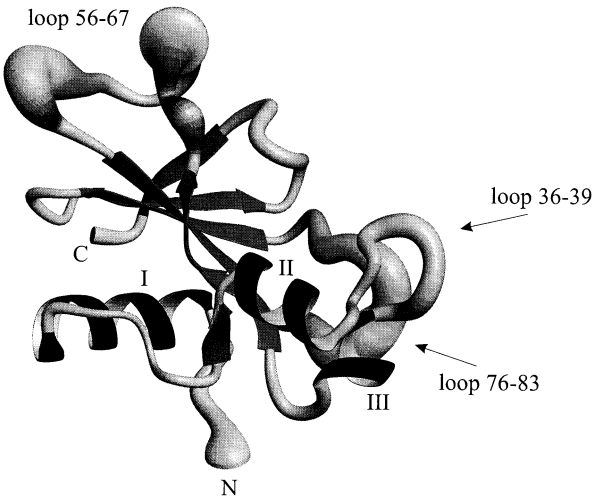

Fig. 2. Schematic presentation of binase spatial structure in solution. Secondary structure elements are shown by ribbons: α-helices are ribbon helices and β-strands are ribbon arrows. The remained regions are shown in 'sausage' representation. The thickness of the sausage is proportional to the atomic root mean square displacement of the corresponding region. α-helices are numbered (I, II, III), loops and N- and C-termini are denoted. The picture was generated with the MOLMOL program [28].

3. Results and discussion

3.1. Binase spatial structure

The used distance and torsion angle constraints as well as some characteristics of the obtained binase structure are summarised in Table 1. Totally, 437 intraresidual, 270 sequential, 72 medium-range, and 124 long-range [19] interproton distance constraints were used in calculations (Fig. 1). Both the DYANA and FANTOM sets of structures are in good agreement with experimental restraints (Table 1). An average pairwise rmsd of the final 20 DYANA (FANTOM) structures is 1.14 ± 0.22 Å (1.25 ± 0.18 Å) for backbone atoms and 1.89 ± 0.22 Å (2.05 ± 0.22 Å) for all heavy atoms, respectively. The rmsd between mean DYANA structure and mean FANTOM structure is 0.89 Å for backbone atoms and 1.17 Å for all heavy atoms.

Binase contains three α-helices and two β-sheets (Fig. 2). Helices I and II (residues 6–16 and 26–32, respectively) are regular: all backbone angles are close to the typical α-helical values. For four backbone amide groups of the residues involved in the α-helices (11, 14, 17 and 29) and exhibiting slow hydrogen-deuterium exchange, the acceptors of hydrogen bonds were not determined unambiguously. For them there were two possibilities to constrain hydrogen bond: NH(i)-CO($i-3$) and NH(i)-CO($i-4$). The single turn of helix III includes residues 41–44 and Ala-45 amide group, which is hydrogen bonded to Leu-41 carbonyl group.

Two β-sheets are found in binase (Fig. 3): five-stranded antiparallel (residues 51–55, 70–75, 86–90, 94–99, and 104–

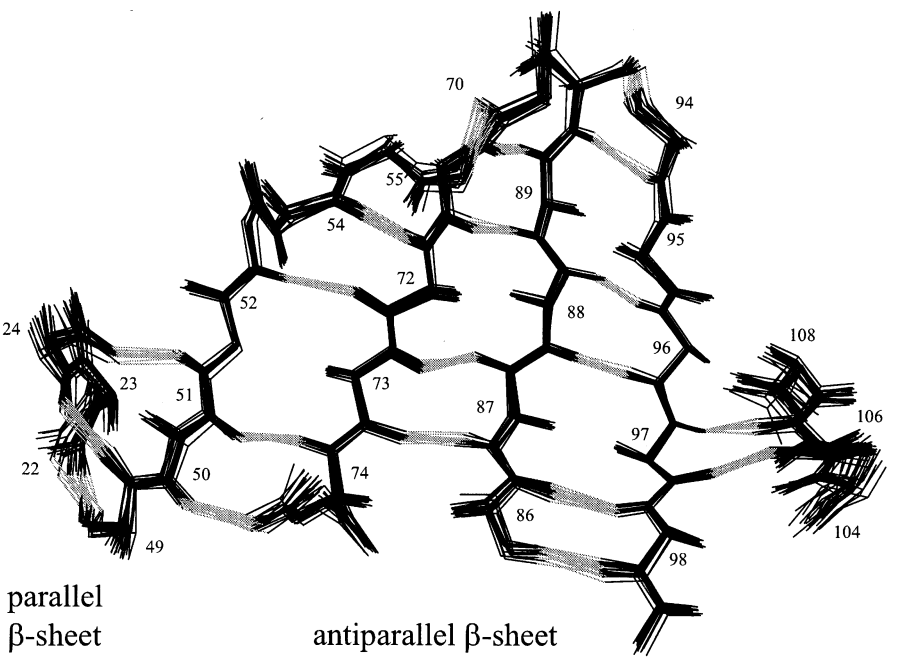

Fig. 3. β-structure of binase. Backbone atoms of β-strand regions of 20 FANTOM structures were superimposed. Backbone is shown in black, hydrogen bonds are in gray.

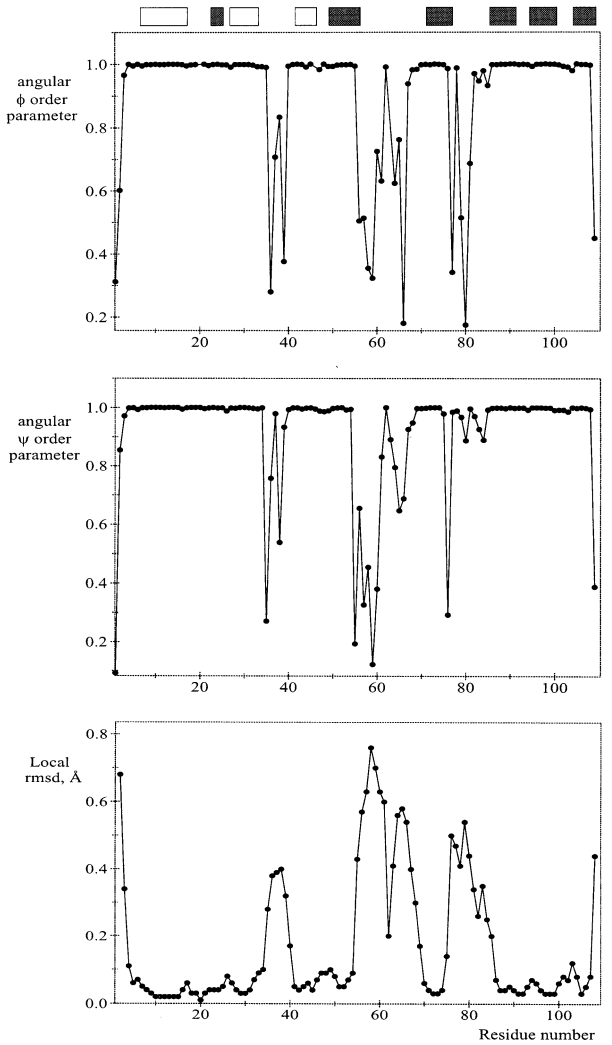

Fig. 4. Angular order parameters and local rmsd of 20 FANTOM structures. Secondary structure elements of binase are shown at the top by rectangles, empty for α-helices and filled for β-strands.

108, strands I–V, respectively) and small two-stranded parallel (residues 22–24 and 49–51). The hydrogen bonding in the antiparallel β-sheet is regular except for the strand I where is a β-bulge of classical type [26], formed by residues Gly-52 and Asp-53. The hydrogen bonds that stabilised the parallel β-sheet are NH(24)-CO(49), NH(49)-CO(22), and NH(51)-CO(24). Strands III and IV of antiparallel β-sheet are connected with type I β-turn (residues 90–93) and strands IV and V are connected with type III′ β-turn (residues 100–103).

The secondary structure elements form two compact regions linked by strand I of antiparallel β-sheet. The first region is composed of strands II, III and IV and packed onto them helix I forming a hydrophobic core of the protein. 45 NOE contacts were observed between side-chain protons in the α/β interface. The hydrophobic side-chain packing within the core is so tight that it causes slow rotation of Tyr-89 aromatic ring [13]. Strands I and V have no contacts with helix I. The second compact region is formed by helices II and III and parallel β-sheet.

Binase has three loops (residues 36–39, 56–67, and 76–83) (Fig. 2). The side-chain of Leu-62 of the 56–67 loop is packed into the hydrophobic 'pocket' formed by Phe-55, Trp-70, Val-88, Tyr-96, Tyr-102 and Phe-105. 17 side-chain/side-chain NOE contacts were detected between these residues and Leu-62. The hydrophobic interactions of Leu-62 hold the orientation of the 56–67 loop relative to the antiparallel β-sheet (Fig. 3).

Backbone torsion angle order parameters [27,28] and local rmsd values (Fig. 4) show that the regions with regular secondary structure are well-defined but loop regions remain undefined (Fig. 3). After the exclusion of two N-terminal and loop residues the rmsd becomes 0.47 ± 0.12 Å (0.65 ± 0.13 Å) for backbone atoms and 1.23 ± 0.15 Å (1.37 ± 0.16 Å) for all heavy atoms of DYANA (FANTOM) structures. The loops along with two N-terminal residues have only a few experimental constraints (Fig. 1). Generally, loops are the worst-defined areas in NMR-derived structures [29]. The lack of experimental data for the binase loops could be explained by high flexibility of these regions.

3.2. Comparison of binase and barnase

The structure of binase in solution is very similar to the crystal structures of binase (3.2 Å resolution, [11]) and binase H101N mutant (2.2 Å resolution, PDB code 2rbi, [12]). Barnase crystal structure [7] (PDB code 1bni) as well as binase crystal structures has a global fold similar to the NMR binase structure. All β-sheets, β-turns and three α-helices are the same in these structures.

Barnase and binase crystal structures contain also a small helix formed by residues 36–38 (here and below we use binase numeration). The corresponding regions of barnase [8] (PDB code 1bnr) and binase in solution are flexible loops. Evidently, crystal packing forces are responsible for the stabilisation of this region.

Binase is more stable than barnase (temperatures of heat denaturation are 56.3 and 54.3°C for binase and barnase, respectively [30], and the difference in free energy of unfolding is 0.93 kcal/mol [5]). The differences in stability and enzymatic activity between barnase, binase, and their mutants and hybrids were analysed being based on crystal structures of binase and barnase. However, as it was discussed above, crystal packing forces essentially affect spatial structures of the proteins and therefore solution structures might be more relevant for the analysis.

The structure of barnase in solution contains only two (I and II) α-helices and five-stranded antiparallel β-sheet. The disrupted helix-like structure in 41–45 region of barnase [8] corresponds to the well-defined α-helix III of binase in solution. The sequences of this region of barnase and binase differ: Asp-43 in barnase is substituted for Glu residue in binase (D43E[1]). Clearly, this substitution stabilises the α-helix III due to disposition of the polar carboxyl group from hydrophobic side-chains of the surrounding residues. Interesting to note is that binase and barnase crystal structures are identical in this region in spite of D43E substitution [5] but an increase of stability of D43E barnase mutant was observed [5] and explained [31].

It was found that a 25–109 hybrid protein (N-terminal part from barnase and residues 25–109 from binase) is an exception from the inverse relationship between thermostability and

[1] Here and below the difference between barnase and binase sequence is designated in the following way: barnase residue, the number of corresponding binase residue, the corresponding binase residue.

enzymatic activity for the barnase-binase hybrids [30,32]. The 25–109 hybrid exhibits binase-like activity because all catalytic and substrate-binding residues [33] of the protein are from binase. The explanation of its lowered thermostability follows from the comparison of the binase and barnase structures in solution rather than in crystal. The residues 22–24 and 49–51, composing parallel β-sheet in binase are the same in barnase, but the β-sheet is not present in barnase in solution [8]. There are four differences nearby the β-sheet (Q14I, T15R, H17K and K18R). Supposing these substitutions to be responsible for the parallel β-sheet stability it is highly probable that the 25–109 hybrid as well as barnase has no parallel β-sheet in solution, which result in its lowered thermostability. The existence of the parallel β-sheet in barnase in crystal [7] is, probably, caused by crystal packing stabilisation.

The residues involved in the catalytic mechanism of binase and barnase [33] are conservative: Glu-72 and Arg-86 in antiparallel β-sheet and His-101 in the β-turn connecting strands IV and V of this β-sheet. In spite of three differences (I87L, L88V and Q103A) nearby the catalytic residues, both X-ray and NMR studies [7,8,12] do not reveal differences between spatial structures of the catalytic site are not able to explain the difference in the enzymatic activities of binase and barnase [5,32].

However, binase and barnase have one more site, crucial for their enzymatic activity and it was found that the most changes in barnase structure caused by substrate [34] and barstar binding [10,35] occur in this region. This is the loop 56–67, which is responsible for substrate binding and takes part in barstar binding with the 'induced fit' mechanism [10,35,36]. The loop is common for microbial ribonucleases and residues Phe-55, Asn-57 and Glu-59, involved in guanine base binding, are strongly conserved [36]. Barnase and binase differ in the sequence of this loop by three residues: K61R, G64S and K65A. The loops 56–67 of binase and barnase in crystal have identical conformations, stabilised by crystal packing forces. In solution in both proteins this loop but Leu-62 residue is poor-defined. It seems that in binase as well as in barnase the loop 56–67 is flexible to provide the induced fit both to substrate and to barstar. Thus an explanation of the differences both in catalysis and in barstar binding of barnase and binase [4,3] would require structural and dynamics data for corresponding complexes.

3.3. Conclusions

The main structure elements and folding of binase and barnase are the same both in crystal and in solution. However, several regions of these proteins differ in solution but are similar in crystal. The differences in thermostability of binase, barnase and their hybrids are explained by the differences in solution structures of binase and barnase. Differences both in enzymatic activity of binase and barnase and in dissociation constants of their complexes with barstar is determined by the differences in the flexible loops. That is why the structural data along with the data on the dynamics of binase, barnase, and their complexes in solution are needed to explain the differences in binase and barnase functioning.

References

[1] Aphanasenko, G.A., Dudkin, S.M., Kaminir, L.B., Leshchinskaya, I.B. and Severin, E.S. (1979) FEBS Lett. 97, 122–125.
[2] Hartley, R.W. and Barker, E.A. (1972) Nature New Biol. 235, 15–16.
[3] Yakovlev, G.I., Moiseyev, G.P., Protasevich, I.I., Ranjbar, B., Bocharov, A.L., Kirpichnikov, M.P., Gilli, R.M., Briand, C.M., Hartley, R.W. and Makarov, A.A. (1995) FEBS Lett. 366, 156–158.
[4] Hartley, Robert W. (1993) Biochemistry 32, 5978–5984.
[5] Serrano, L., Day, A.G. and Fersht, A.R. (1993) J. Mol. Biol. 233, 305–312.
[6] Maugen, Y., Hartley, R.W., Dodson, E.J., Dodson, G.G., Bricogne, G., Chothia, C. and Jack, A. (1982) Nature 297, 162–164.
[7] Buckle, A.M., Henrick, K. and Fersht, A.R. (1993) J. Mol. Biol. 234, 847–860.
[8] Bycroft, M., Ludvigsen, S., Fersht, A.R. and Poulsen, F.M. (1991) Biochemistry 30, 8697–8701.
[9] Lubienski, M.J., Bycroft, M., Freund, S.M. and Fersht, A.R. (1994) Biochemistry 33, 8866–8877.
[10] Buckle, A.M., Schreiber, G. and Fersht, A.R. (1994) Biochemistry 33, 8878–8889.
[11] Pavlovsky, A.G., Vagin, A.A., Vainstein, B.K., Chepurnova, M.K. and Karpeisky, M.Ya. (1983) FEBS Lett. 162, 167–170.
[12] Okorokov, A.L., Panov, K.I., Offen, W.A., Mukhortov, V.G., Antson, A.A., Karpeisky, M.Ya., Wilkinson, A.J. and Dodson, G.G. (1997) Protein Eng. 10, 273–278.
[13] Reibarkh, M.Ya., Nolde, D.E., Bocharov, E.V., Vasil'eva, L.I., Shulga, A.A., Kirpichnikov, M.P. and Arseniev, A.S. (1997) Russ. J. Bioorg. Chem. 23, 706–717.
[14] Schulga, A.A., Okorokov, A.L., Panov, K.I., Kurbanov, F.T., Chernov, B.K., Skryabin, K.G. and Kirpichnikov, M.P. (1994) Mol. Biol. (Russ.) 28, (2) 303–310.
[15] Jeener, J., Meier, G.H., Bachman, P. and Ernst, R.R. (1979) J. Chem. Phys. 71, 4546–4553.
[16] Rance, M., Sorensen, O.W., Bodenhausen, G., Wagner, C., Ernst, R.R. and Wuthrich, K. (1983) Biochem. Biophys. Res. Commun. 117, 479–485.
[17] Kay, L.E. (1995) Prog. Biophys. Mol. Biol. 63, 277–299.
[18] Bartels, C., Xia, T.-H., Billeter, M., Guntert, P. and Wuthrich, K. (1995) J. Biomol. NMR 6, 1–10.
[19] Guntert, P., Mumenthaler, C. and Wuthrich, K. (1997) J. Mol. Biol. 273, 283–298.
[20] Yang, A.S. and Honig, B. (1995) J. Mol. Biol. 252, 366–376.
[21] Baker, E.N. and Hubbard, R.E. (1984) Prog. Biophys. Mol. Biol. 2, 97–179.
[22] Szyperski, T., Guntert, P., Otting, G. and Wuthrich, K. (1992) J. Magn. Res. 99, 552–560.
[23] Bystrov, V.F. (1976) Prog. NMR spectrosc. 10, 41–81.
[24] Arseniev, A., Schultze, P., Worgotter, E., Braun, W., Wagner, G., Vasak, M., Kagi, J.H.R. and Wuthrich, K. (1988) J. Mol. Biol. 201, 637–657.
[25] Schaumann, T., Braun, W. and Wuthrich, K. (1990) Biopolymers 29, 679–694.
[26] Richardson, J.S. (1981) Adv. Protein Chem. 34, 167–339.
[27] Hyberts, S.G., Goldberg, M.S., Havel, T.F. and Wagner, G. (1992) Protein Sci. 1, 736–751.
[28] Koradi, R., Billeter, M. and Wuthrich, K. (1996) J. Mol. Graph. 14, 51–55.
[29] Clore, G.M., Gronenborn, A.M., Kjaer, M. and Poulsen, F.M. (1989) Protein Eng. 1, 305–311.
[30] Ranjbar, B., Protasevich, I.I., Shulga, A.A., Kurbanov, F.T., Lobachev, V.M., Kirpichnikov, M.P. and Makarov, A.A. (1997) Mol. Biol. (Russ.) 31, 492–499.
[31] Golovanov, A.P., Efremov, R.G., Jaravine, V.J., Vergoten, G., Kirpichnikov, M.P. and Arseniev, A.S. (1998) J. Biomol. Struct. Dyn. 15, 673–687.
[32] Kurbanov, F.T., Shulga, A.A., Ranjbar, B., Makarov, A.A. and Kirpichnikov, M.N. (1997) Mol. Biol. (Russ.) 31, 1057–1063.
[33] Hill, C., Dodson, G., Heinemann, U., Seanger, W., Mitsui, Y., Nakamura, K., Borisov, S., Tischenko, G., Polyakov, K. and Pavlovsky, S. (1983) Trends Biochem. Sci. 8, 364–369.
[34] Meiering, E.M., Bycroft, M., Lubienski, M.J. and Fersht, A.R. (1993) Biochemistry 32, 10975–10987.
[35] Jones, D.N.M., Bycroft, M., Lubienski, M.J. and Fersht, A.R. (1993) FEBS Lett. 331, 165–172.
[36] Sevcik, J., Sanishvili, R.G., Pavlovsky, A.G. and Polyakov, K.M. (1990) Trends Biochem. Sci. 15, 158–162.